Bioorganic Chemistry 92 (2019) 103293

Contents lists available at ScienceDirect

Bioorganic Chemistry

journal homepage: www.elsevier.com/locate/bioorg

Umbelliferone derivatives exert neuroprotective effects by inhibiting monoamine oxidase A, self-amyloidβ aggregation, and lipid peroxidation

Su Hui Seong[a], Md Yousof Ali[b,c], Hyun Ah Jung[d,**], Jae Sue Choi[a,*]

[a] Department of Food and Life Science, Pukyong National University, Busan 48513, Republic of Korea
[b] Department of Chemistry and Biochemistry, Faculty of Arts and Science, Concordia University, 7141 Sherbrooke St. W., Montreal, Quebec, Canada
[c] Centre for Structural and Functional Genomic, Department of Biology, Faculty of Arts and Science, Concordia University, 7141, Sherbrooke St. W., Montreal, Quebec, Canada
[d] Department of Food Science and Human Nutrition, Chonbuk National University, Jeonju 54896, Republic of Korea

ARTICLE INFO

Keywords:
6-Formyl umbelliferone
MAO-A
Neuropsychiatric disorder
Enzyme kinetics
Computational docking
Aβ self-aggregation

ABSTRACT

Umbelliferone has been demonstrated to have a wide range of biological activities. However, the effect of incorporating a formyl moiety in the umbelliferone scaffold has not been investigated. In this paper, we investigated the inhibitory activity of six coumarins, namely umbelliferone (**1**), 6-formyl umbelliferone (**2**), 8-formyl umbelliferone (**3**), umbelliferone-6-carboxylic acid (**4**), esculetin (**5**), and scopoletin (**6**) against human monoamine oxidases (*h*MAOs), self-amyloid β (Aβ) aggregation, and lipid peroxidation. We found that all compounds had high selectivity for *h*MAO-A in comparison with *h*MAO-B. Among the compounds, **2** exhibited the highest *h*MAO inhibitory activity with an IC_{50} value of 3.23 μM for *h*MAO-A and 15.31 μM for *h*MAO-B. Enzyme kinetic analysis showed that **2** and **3** were competitive *h*MAO inhibitors. In silico hydrated molecular docking simulations revealed that the coumarins interacted with substrate-binding site residues of the enzymes and the isoalloxazine ring of FAD. In addition, formyl coumarins **2** and **3** significantly inhibited lipid peroxidation in rat brain homogenates and self-$A\beta_{25-35}$ aggregation compared to other derivatives. These represent the first experimental and modelling data for *h*MAO-A/B inhibition by umbelliferone derivatives. Together, the data suggest that introduction of a formyl moiety in the 7-hydroxycoumarin scaffold, especially at the 6 position, plays an important role in the inhibition of *h*MAOs, Aβ self-aggregation, and lipid peroxidation. Umbelliferone derivative **2** is a promising therapeutic lead scaffold for developing anti-neuropsychiatric disorder drugs that function via selective *h*MAO-A inhibition.

1. Introduction

Monoamine oxidases (MAO, EC 1.4.3.4) are flavoproteins located at the outer mitochondrial membrane in neuronal, astroglial, and other cells, and are considered therapeutic targets for the treatment of neurodegenerative and neuropsychiatric disorders [1,2]. These enzymes catalyze the inactivation of biogenic and xenobiotic monoamines, which are neurotransmitters [3]. There are two isoforms of MAO, MAO-A and MAO-B, which share 70% sequence identity, but each enzyme has different substrate affinities: MAO-A selectively breaks down dopamine, serotonin and norepinephrine whereas MAO-B breaks down dopamine, phenethylamine, and benzylamine. Both isoforms equally break down tyramine and dopamine [4].

In addition, MAO activation increases the production of reaction products, including hydrogen peroxide (H_2O_2), which may further produce free radicals [5]. Several experimental studies have demonstrated that MAO-A and MAO-B could be major sources of H_2O_2 in the aging heart and brain, respectively [6,7]. Therefore, development of MAO inhibitors (MAOIs) are important not only for treatment of symptoms by up-regulating the half-life of monoamines, but also for neuroprotection via inhibition of H_2O_2 [8].

Selective MAO-A inhibitors (clorgyline and moclobemide) and non-selective MAOIs are used to treat depression and anxiety, while selective MAO-B inhibitors (selegiline and rasagiline) are used as anti-Parkinson's disease or anti-Alzheimer's disease agents. However, non-selective irreversible MAOIs, such as tranylcypromine, can potentiate the cardiovascular effects (cheese effect) of dietary tyramine [2]. Thus, selective reversible inhibition of MAO-A or MAO-B are desirable, although irreversible MAOIs are still prescribed as antidepressants with dietary control. Although various kinds of MAOIs have been discovered and used

* Corresponding author at: Department of Food and Life Science, Pukyong National University, Busan 48513, Republic of Korea.
** Corresponding author at: Department of Food Science and Human Nutrition, Chonbuk National University, Jeonju 54896, Republic of Korea.
E-mail addresses: jungha@jbnu.ac.kr (H.A. Jung), choijs@pknu.ac.kr (J.S. Choi).

https://doi.org/10.1016/j.bioorg.2019.103293
Received 27 May 2019; Received in revised form 9 September 2019; Accepted 16 September 2019
Available online 18 September 2019
0045-2068/

to treat neuronal disorders, utilization of MAOIs is limited by side effects such as sleep disturbances and anxiety (moclobemide), anorexia, dry mouth, and orthostatic hypotension (selegiline), and hypertensive crisis (tranylcypromine) [9]. Due to these adverse drug reactions, a good understanding of the pharmacokinetics and pharmacodynamics of MAOIs is very important and could result in improved treatment of patients in the future. Natural products such as flavonoids, tea catechins, and silymarin have been proposed as new lead MAOIs; these exert neuroprotective effects via reducing reactive oxygen species [10,11]. Interestingly, quercetin inhibited MAO-A activity in mouse brain cells without impacting intestinal MAO-A activity, indicating that it is safe MAO-A inhibitor compared to other synthetic drugs [10]. Therefore, naturally occurring products and their active ingredients represent a valuable resource for structure-based drug design and the development of safe treatments for depressive and neurodegenerative disorders.

Aggregation of amyloidβ (Aβ) peptides is also closely related to the pathogenesis of various kinds of neurodegenerative disease. Aβ plaques can induce oxidative stress in neurons through the formation of hydrogen peroxide (H_2O_2) [12,13]. A previous study reported that aggregated Aβ peptides are directly toxic to cultured neurons, whereas Aβ peptides in a soluble state lack direct toxicity [14].

Coumarins, which have a 1-benzopyran-2-one scaffold, are an important group of organic compounds derived from synthetic and natural sources. Coumarins are widely distributed in plants and are abundant in the plant families Apiaceae, Rutaceae, and Umbelliferae [15]. Thus far, more than 1300 natural coumarins have been identified and these coumarins have diverse pharmacological effects including anti-coagulant [16], anti-inflammatory [17], anti-viral [18], neuroprotective [19], and anti-cancer activities [20]. Of great interest is their strong effects on the central nervous system (CNS). Many coumarins from natural and synthetic sources have been reported to have cholinesterase and MAO inhibitory effects [15]. In addition, the simple coumarin, scopoletin (**6**), showed anti-depression activity via activation of dopamine D_1 and D_2 receptors [21].

Previous studies have shown that administration of umbelliferone (**1**) and **5** significantly attenuated 1-methyl-4-phenyl-1,2,3,6-tetrahydropyridine (MPTP)-induced neurotoxicity in an animal model by preventing apoptosis and increasing glutathione levels, whereas these compounds did not inhibit MAO activity [22]. In our previous study, 6-formyl umbelliferone (**2**) and 8-formyl umbelliferone (**3**) showed anti-Alzheimer's disease activity via noncompetitive inhibition of BACE1 *in vitro* [23]. Recently, Qin et al. reported that **1** showed anti-depressant activity via modulation of the Rho-associated protein kinase/Akt pathway [24]. Thus, coumarins are potentially valuable resources for the treatment of neuronal disorders such as Parkinson's disease, anxiety, depression, and Alzheimer's disease.

Here, as part of our ongoing goal to discover multi-target-directed ligands of natural origin that may have the potential to treat CNS disorders, we investigated the ability of coumarins **1** and **2**, umbelliferone-6-carboxylic acid (**4**) isolated from *Angelica decursiva*, 8-formyl umbelliferone (**3**) synthesized from coumarin **1**, esculetin (**5**), and scopoletin (**6**) to inhibit *h*MAO-A and B, self-Aβ aggregation, and lipid peroxidation. We studied the structure-activity relationship between umbelliferone derivatives that possess different functional groups at the C-6 or C-8 positions of the umbelliferone scaffold and performed hydrated docking analysis to determine the mechanism of *h*MAO inhibition by umbelliferone derivatives (**1–6**) and the role of water molecules in inhibitor binding to *h*MAOs.

2. Results and discussion

2.1. In vitro hMAO A and B inhibitory activities of the coumarins

Many coumarin derivatives of synthetic or natural origin have been reported to be MAOIs with high selectivity towards type-B MAO [25]. The substituent at the C7 position of the coumarin scaffold is crucial for selectivity towards type-A or -B isoforms [26]. Coumarin **1** was reported to have an IC_{50} value of 87.5 μM for inhibition of MAO in mouse brain [27]. Gnerre et al. demonstrated that introduction of a lipophilic moiety, such as a methyl or benzyloxy group in 7-hydroxycoumarin (umbelliferone, **1**), significantly increased MAO inhibitory activity, whereas introduction of a glucose moiety in the C6 position abolished inhibitory activity [25]. In another study, Lee et al. reported that 6,7-dihydroxycoumarin (esculetin) was 1.5 times more active than 7-hydroxy-6-methoxycoumarin (scopoletin) in inhibiting mouse brain MAO [28]. However, the effect of a formyl group in the umbelliferone scaffold on MAO inhibition has not previously been explored.

In the present study, coumarins (**1–6**) were tested *in vitro* for their *h*MAO-A and *h*MAO-B inhibitory activities using R-(–)-deprenyl HCl as a reference drug. The results of the luminescence assay revealed that coumarin **1**, the representative constituent of *A. decursiva*, showed moderate inhibitory potency against both *h*MAO-A and B with IC_{50} values of 39.16 ± 0.85 and 147.37 ± 3.65 μM, respectively. Introduction of a formyl moiety into the umbelliferone scaffold dramatically increased inhibitory potency. Coumarin **2,** which possess a formyl moiety in the C-6 position of umbelliferone, was the most potent *h*MAO-A and *h*MAO-B inhibitor with IC_{50} values of 3.23 ± 0.42 and 15.31 ± 0.42 μM, respectively.

To understand the role of the formyl moiety and its position in the umbelliferone scaffold on *h*MAO inhibition, we further investigated the anti-*h*MAO activity of **3–6**. A change in position of the formyl moiety from C-6 to C-8 resulted in a significant drop in both *h*MAO-A and -B inhibition (IC_{50} of **3**: 10.46 ± 0.94 μM for *h*MAO-A and 81.35 ± 2.59 μM for **3**). In addition, introduction of hydroxyl, methoxyl, and carboxyl moieties in the C-6 position of the umbelliferone scaffold decreased the inhibitory activity against *h*MAO-A (IC_{50} values of **4–6**: 100.24 ± 6.40, 122.53 ± 0.58, and 207.65 ± 1.91 μM, respectively). In the case of *h*MAO-B, introduction of a carboxyl moiety in the C-6 position of the umbelliferone scaffold did not affect the inhibitory activity, whereas introduction of hydroxyl and methoxyl moieties significantly decreased the inhibitory potency (IC_{50} of **4**: 144.27 ± 5.52 μM). Contrary to R-(–)-deprenyl HCl, a selective MAO-B inhibitor with a selective index (SI) of 88.5, **1–6** were exceptionally selective *h*MAO-A inhibitors with SI values of less than 0.69.

Overall, these results indicate that the formyl group in the 7-hydroxycoumarin scaffold plays an important role in the inhibition of MAOs compared to other functional moieties such as hydroxyl, methoxyl, and carboxyl groups.

2.2. Kinetic parameters of hMAO A and B inhibition

To investigate the *h*MAO inhibition mechanism, we analyzed enzyme kinetics and obtained Lineweaver-Burk plots and secondary plots of slopes (K_{mapp}/V_{maxapp}) and $1/V_{maxapp}$ versus concentrations of coumarins **2** and **3** (Table 1). Double reciprocal Lineweaver-Burk plots for the inhibition of *h*MAO-A and *h*MAO-B by compounds **2** and **3** were linear and intersected on the y-axis (Fig. 1A, C, 2A and C), indicating that **2** and **3** are competitive inhibitors of *h*MAO-A and *h*MAO-B. Inhibition constants (K_i) for *h*MAO-A and *h*MAO-B inhibition were calculated to be 3.05 and 6.81 μM for compound **2** and 11.04 and 20.42 μM for compound **3**, respectively, based on secondary plots of slopes versus [inhibitor]. In addition, secondary plots of $1/V_{maxapp}$ versus [inhibitor] were parallel to the *x*-axis without changes in the V_{max} value (Fig. 1B, D, 2B and D). These enzyme kinetic results imply that coumarins **2** and **3** bind free *h*MAO, not the enzyme-substrate complex. In other words, these coumarins compete with the substrate and interact with the catalytic site of *h*MAOs, not the allosteric site of *h*MAOs.

2.3. In silico hydrated docking simulations of coumarins to hMAO-A and B

To validate and optimize the molecular docking protocol, we re-docked native co-ligands (harmine for *h*MAO-A and safinamide for

Table 1

Recombinant human monoamine oxidase (*h*MAO) inhibitory activity of coumarins.

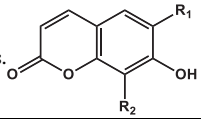

	R_1	R_2	IC_{50} (μM)[a]		SI[b]	Inhibition type	K_i value (μM)
			*h*MAO-A	*h*MAO-B			
1	H	H	39.16 ± 0.85	147.37 ± 3.65	0.27	–	–
2	CHO	H	3.23 ± 0.42	15.31 ± 0.68	0.21	C[c], C[d]	3.05[e], 6.81[f]
3	H	CHO	10.46 ± 0.94	81.35 ± 2.59	0.13	C[c], C[d]	11.04[e], 20.42[f]
4	COOH	H	100.24 ± 6.40	144.27 ± 5.52	0.69	–	–
5	OH	H	122.53 ± 0.58	> 300	< 0.41	–	–
6	OCH_3	H	207.65 ± 1.91	> 300	< 0.69	–	–
Positive control[g]	–	–	8.85 ± 0.07	0.10 ± 0.01	88.5	–	–

(–) Not tested, *C* Competitive.

[a] Values are expressed as the mean ± SD, $n = 3$.

[b] Selective index (SI) was calculated as the ratio of *h*MAO-A IC_{50}/*h*MAO-B IC_{50}.

[c,e] *h*MAO-A inhibition type was determined by Lineweaver Burk plot and inhibition constant was determined by a secondary plot.

[d,f] *h*MAO-B inhibition type and inhibition constant.

[g] Positive control, R-(–)-deprenyl HCl.

*h*MAO-B) into the catalytic site of *h*MAO-A/B to assess the root-mean-square deviation (RMSD) value between our hydrated docking results and the original crystallographic structures of the target enzymes. Harmine, a β-carboline derivative, is a reversible selective MAO-A inhibitor with a K_i value of 5 nM [29], while safinamide is a potent, selective, and reversible MAO-B inhibitor with a K_i value of 0.45 μM [30]. The best positions of harmine and sulfonamide generated by AutoDock 4.2 for *h*MAO-A (2z5x) and *h*MAO-B (2v5z) correlated well with the crystallographic binding results (RMSD values of < 1.0 Å). This validated docking protocol was used to investigate the binding of coumarins to *h*MAOs.

The active site of MAOs has an FAD-binding site, substrate-binding site (SBS), and specific sites that determine the selectivity of inhibitors. Lys305 and Trp397 in *h*MAO-A and Lys296 and Trp388 in *h*MAO-B are important for the activity of *h*MAOs and play a crucial role in the non-covalent binding of FAD [31]. It was established that Tyr407 and Tyr444 in the A isoform and Tyr398 and Tyr435 in the B isoform are important for stabilizing substrate binding through formation of aromatic sandwich interactions between enzyme and substrate [8].

As shown in Fig. 3, coumarins **1**–**6** could be docked into the catalytic active site of *h*MAO-A with negative binding energies (see Table 2). In the compound **2**-*h*MAO-A complex (Fig. 3B), Tyr444 and Tyr197 residues and the formyl moiety of **2** were bridged by H-bonds provided by one water molecule. Phe352 and Tyr407 residues were involved in hydrophobic interactions with **2** via pi-pi *T*-shaped and pi-pi stacked interactions, respectively. In addition, **2** engaged in van der Waals interactions with FAD. In the compound **3**-*h*MAO-A complex (Fig. 3C), the isoalloxazine ring of FAD bound the oxygen atom in the ketone moiety of **3** via a water-mediated pi-donor H-bond. In addition, **3** interacted with Tyr407 (pi-pi stacked), Ile180 (pi-alkyl), and Ile335 (pi-

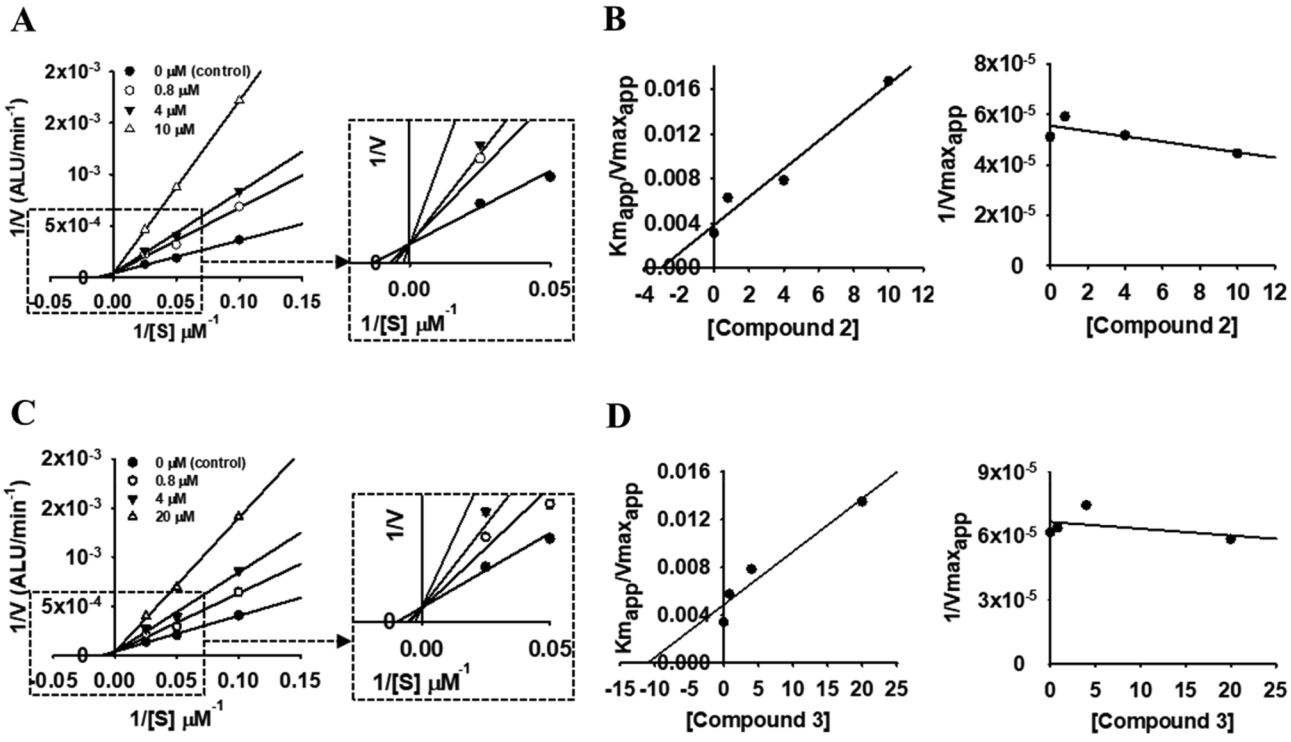

Fig. 1. Lineweaver-Burk plots and secondary plots of **2** (A and B) and **3** (C and D) for *h*MAO-A inhibition.

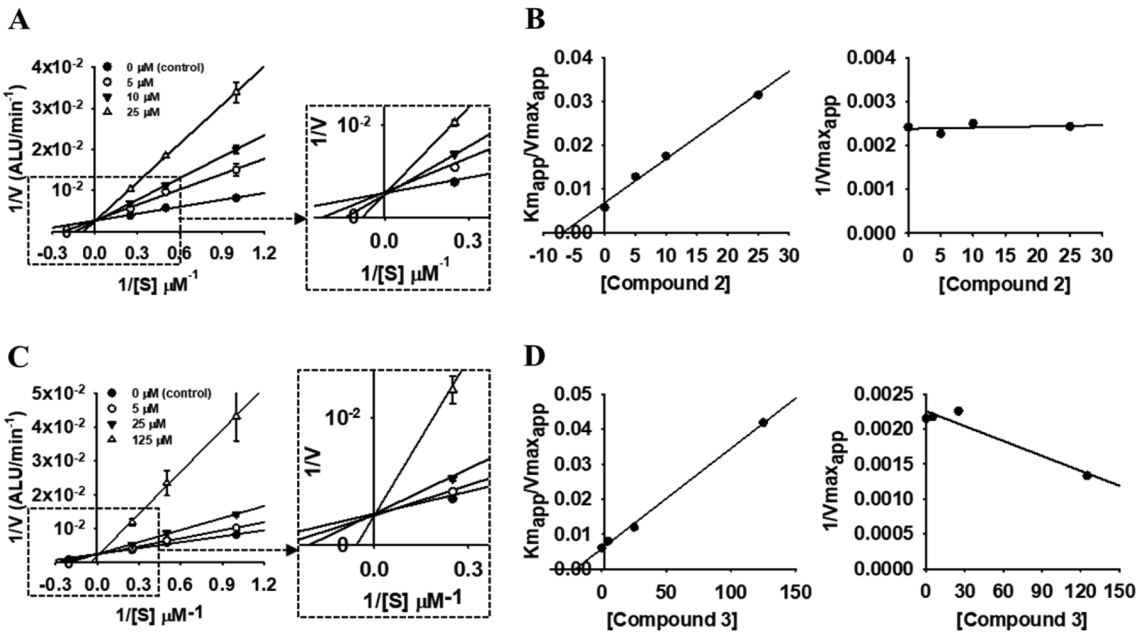

Fig. 2. Lineweaver-Burk plots and secondary plots of **2** (A and B) and **3** (C and D) for *h*MAO-B inhibition.

alkyl) via hydrophobic interactions. As shown in Fig. 3A, 1 interacted with tyrosine residues at positions 407 and 444 of the substrate-binding site (SBS) via pi-pi stacked aromatic sandwich interactions. In addition, hydroxyl and ketone moieties of **1** formed direct H-bonds with FAD and Tyr197 residues.

These docking results are in agreement with previous reports that the aromatic parts of *h*MAO SBS residues are more essential for enzyme activity than the hydroxyl parts. The hydroxyl moiety of Tyr444 (Tyr435 for *h*MAO-B) is more important than that of Tyr407 for binding of substrate to *h*MAO-A (Tyr398 for *h*MAO-B) [31]. The pi-pi interactions formed by SBS residues could play an important role in the inhibitory activity of coumarins **1**, **2**, and **3** toward *h*MAO-A and their inhibitory effects. Coumarins **4**–**6** had limited hydrophobic and hydrophilic interactions with the SBS residues of *h*MAO-A, although they did form several direct H-bonds or water-mediated H-bonds with residues.

Similar to the docking results for *h*MAO-A, umbelliferones **1**–**3** were surrounded by aromatic sandwich interactions formed by SBS residues of *h*MAO-B including Tyr398 and Tyr435. In addition, the formyl moiety of **2** interacted directly with the isoalloxazine ring of FAD via a C—O bond and hydrophobic interactions (pi-pi *T*-shaped and Pi-lone pair) (Fig. 4B), but the formyl moiety of **3** formed a water-mediated H-bond with Thr399, which is not in the active site of *h*MAO-B (Fig. 4C), which may explain the difference in *h*MAO-B inhibitory activity between **2** and **3**. As shown in Fig. 4A, 1 had limited interaction with FAD. In the case of the **4**-*h*MAO-B complex, **4** was not surrounded by aromatic sandwich interactions (Fig. 4D).

In accordance with the *in vitro* enzyme activity, both **2** and **3** interacted with Ile335 of *h*MAO-A, which is an important *h*MAO-A residue for inhibitor selectivity, but did not interact with Tyr326 of *h*MAO-B, which is essential for *h*MAO-B selectivity [32]. As shown in Table 3, the activating *h*MAO-B ligands deprenyl and sulfinamide formed hydrophobic interactions with Tyr326.

In addition, the crystal structures of *h*MAOs in complex with coumarins **2** or **3** revealed that they all bound non-covalently to the enzyme, which is a desirable property to minimize side effects. In addition, water molecules acted as bridges between the active site residues and coumarins via formation of water-mediated H-bonds. However, these water molecules could also act as blockers for ligands by disturbing the interaction between the ligand and the active site residues of the enzyme.

2.4. Inhibitory effect of coumarins on the formation of $A\beta_{25-35}$ fibrils

Six coumarins and a known inhibitor of $A\beta_{25-35}$ aggregation, curcumin, were assayed for their ability to inhibit self $A\beta_{25-35}$ aggregation using the thioflavin-T fluorometric method. As shown in Table 4, curcumin and coumarin **3** inhibited $A\beta_{25-35}$ fibril formation with IC_{50} values of 6.59 ± 0.27 and 75.57 ± 1.62 μM, respectively. At 100 μM, coumarins **2** and **3** inhibited $A\beta_{25-35}$ aggregation by 25.98 and 64.77%, respectively. However, the other coumarins did not show any inhibitory activity at the tested concentration. This result implies that coumarins with a formyl moiety bind more strongly to $A\beta_{25-35}$ aggregates than those without. Therefore, the formyl moiety appears to be crucial for high affinity binding.

There is substantial evidence that abnormal self-aggregation of Aβ plays a role in the pathogenesis of several CNS diseases, including Alzheimer's disease and depression [12]. Due to the fact that many factors may cause Aβ aggregation, we decided to test our coumarins in a self-aggregation assay. The experimental data presented in this paper showed that **2** and **3**, which possess a formyl moiety, inhibited the aggregation of $A\beta_{25-35}$ *in vitro*, with the presence of a formyl moiety in the C-8 position of the umbelliferone scaffold inhibiting self-$A\beta_{25-35}$ aggregation significantly more than a formyl moiety in the C-6 position. This inhibitory action may cause the Aβ peptide to remain in the soluble monomer state and thereby facilitate clearance of the peptide from the brain through normal physiologic mechanisms [33].

2.5. Inhibitory effect of coumarins on lipid peroxidation in rat brain homogenates

We evaluated the antioxidant activity of coumarins by evaluating their ability to inhibit lipid peroxidation in Fe^{2+}-treated rat brain homogenates. In the stimulated control group, TBAR level was significantly increased compared to the blank group ($p < 0.001$), as shown in Table 4. Among the tested coumarins, **2**, **3**, and **5** dose-dependently inhibited Fe^{2+}-induced lipid peroxidation with EC_{50} values of 8.98 ± 1.03, 7.22 ± 1.67, and 22.78 ± 4.42 μM, respectively. As shown in Fig. 5, coumarins **2** and **3** had more potent inhibitory activity than the positive control, trolox, at 12.5 μM. However, coumarins **1**, **4**, and **6** did not affect TBAR levels at the tested concentration (25 μM).

In the brain, MAOs and Aβ plaques could be major sources of H_2O_2

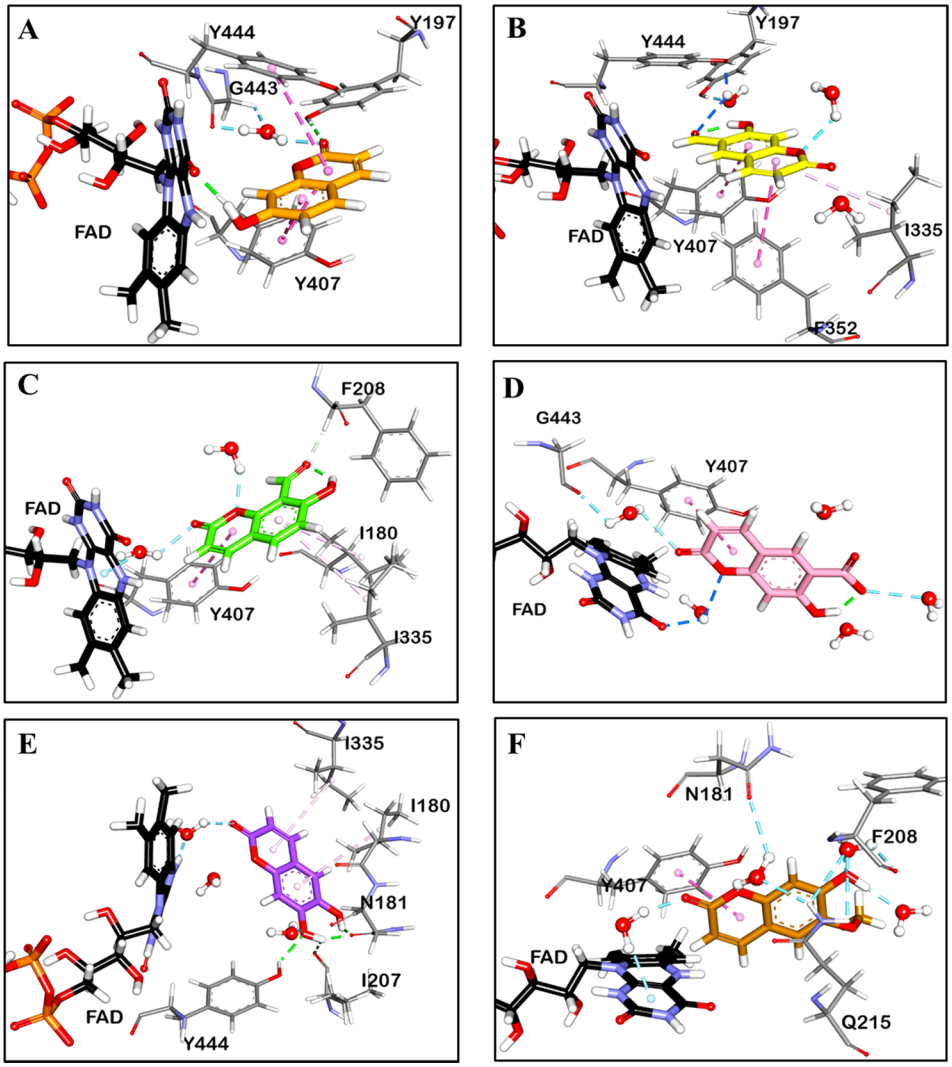

Fig. 3. Binding orientation of compounds **1–6** (A–F) in the catalytic site of *h*MAO-A (PDB: 2z5x). Compounds **1**, **2**, **3**, **4**, **5**, **6**, and FAD are represented by orange, yellow, green, pink, purple, brown, and black sticks, respectively. Water molecules are represented by scaled balls and sticks. H-bonds, water H-bonds pi-pi interactions, and pi-alkyl interactions are shown by green, blue, pink, and pale pink dashed lines, respectively.

[5,13]. The combination of hydrogen peroxide and Fe^{2+} (Fenton's reagent) is used to initiate lipid peroxidation [34]. Coumarins **2**, **3**, and **5** significantly reduced TBAR formation in rat brain tissue homogenate. However, **1**, **4**, and **6** showed no effect at the tested concentration. Our results are consistent with the findings of Thuong et al., who demonstrated that **1** and **6** showed no or low activity against Fe^{2+}/ascorbic acid-induced lipid peroxidation, whereas **5** markedly inhibited lipid peroxidation with an IC_{50} value of 9.6 μM [35]. This result indicates that the formyl and catechol groups of coumarins contribute markedly to their anti-lipid peroxidation properties.

Table 2
Molecular interaction of *h*MAO-A (2z5x) active site with coumarins **1–6** as well as a reported inhibitor.

Compound	Total binding energy[a]	H-bond interaction		Other interaction residues
		Direct	Water mediated	
1	–7.67	FAD, Tyr197	Gly443	Tyr407, Tyr444 (pi-pi stacked)
2	–8.45	–	Tyr444, Tyr197	Tyr407 (pi-pi stacked), Phe352 (pi-pi *T*-shaped), Ile335 (pi-alkyl), FAD (van der Waals)
3	–9.23	–	FAD	Ile180 and Ile335 (pi-alkyl), Tyr407 (pi-pi stacked), Phe208 (C—O bond)
4	–8.51	–	Gly443, FAD	Tyr407 (pi-pi stacked)
5	–8.32	Tyr444, Asn181, Ile207	Tyr444, FAD, Ile207,	Ile335 and Ile180 (pi-alkyl)
6	–8.21	–	FAD, Asn181, Gln215, Phe208	Tyr407 (pi-pi stacked)
Harmine[b]	–8.43	–	FAD, Gly443, Tyr197	Ile335, Tyr407, Tyr444, and FAD (pi-alkyl), Tyr407 (pi-pi stacked), Asn181 (C—O bond)

[a] Total binding energy (kcal/mol) of the hydrated inhibitor was calculated as the sum of normal ligand and W atom potentials.
[b] Reported inhibitor.

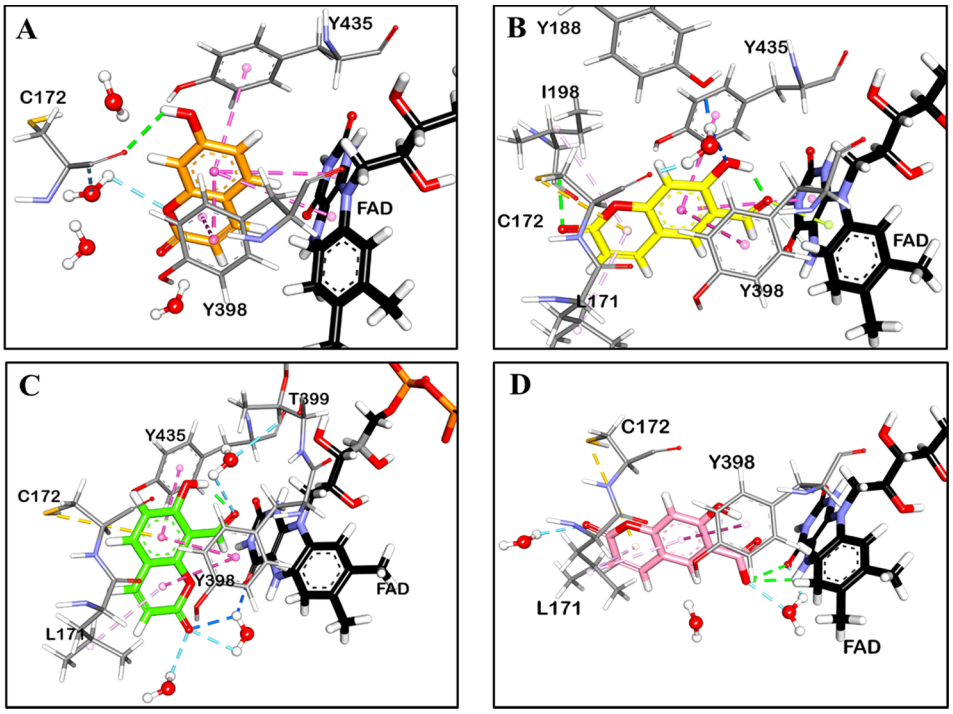

Fig. 4. Binding orientation of compounds **1–4** (A–D) in the catalytic site of *h*MAO-B (PDB: 2v5z). Compounds **1**, **2**, **3**, **4**, and FAD are represented by orange, yellow, green, pink, and black sticks, respectively. Water molecules are represented by scaled balls and sticks. H-bonds, water H-bonds, pi-pi interactions, pi-alkyl interactions, and pi-sulfur interactions are shown by the green, blue, pink, pale pink, and yellow dashed lines, respectively.

2.6. Prediction of pharmacokinetic parameters

Apart from strong *h*MAO-A/B inhibitory activity, the most vital requirements for a successful CNS drug are to penetrate and reach the target protein. PreADMET predicts the values of physically relevant descriptors and pharmaceutically important properties of drug candidates, which can then be compared with recommended values of ideal drugs [36–39]. Predicted pharmacokinetic values of compounds **1–3** along with appropriate reference ranges are presented in Table 5. Log $P_{o/w}$ is commonly used as a reliable index of the lipophilicity of a drug candidate. Log $P_{o/w}$ values of compounds **1–6** were 1.44, 1.44, 1.19, 1.60, 1.54, and 1.68, respectively. HIA is the sum of bioavailability and absorption evaluated from the ratio of excretion or cumulative excretion in urine, bile, and feces [40]. HIA data showed that compounds **1**, **2**, **3**, and **6** are likely to be well absorbed, making these coumarins suitable for oral delivery [37]. However, HIA data indicated that coumarins **4** and **5** would only be moderately absorbed. Binding of a drug to plasma proteins can influence the drug's biological half-life. As shown in Table 4, compounds **1–6** possess 42.39, 81.58, 54.96, 83.93, 11.47, and 29.42% PPB. BBB penetration values provide information about the therapeutic potential of drugs in the CNS. BB values of compounds **1–3** were 0.59, 0.69, and 0.69, respectively. Compounds **1–4** and **6** were not predicted to be CYP2D6 and CYP3A4 inhibitors, whereas compound **5** was predicted to be a CYP3A4 inhibitor. These predictions of drug-likeness suggested that compounds **2–3**, and **6** have suitable drug-like properties according to CMC-like [41] and Lipinski's rules [42]. Coumarins **1** and **5** do not have a qualified structure according to the CMC-like rule, but they do have a suitable structure according to Lipinski's rule.

Hydrophobic interactions may play a critical role in the effectiveness of compounds at inhibiting mitochondrial MAO-A and B activity because these enzymes are located at the outer mitochondrial membrane [10]. Log $P_{o/w}$ is commonly used as a reliable index of the lipophilicity of a drug candidate. As shown in Table 5, predicted log $P_{o/w}$ values indicated that coumarins **1–6** have moderate hydrophobicity; in particular, introduction of a methoxyl group in the umbelliferone scaffold increased lipophilicity markedly. ADMET predictions were that compounds **1–6** can be absorbed into the CNS, have moderate BBB penetration, and only bind plasma proteins weakly. A low PPB value is normally regarded to be important [43]. Interestingly, introduction of a formyl moiety significantly enhanced the BBB penetration value. The results of drug-likeness prediction, including Lipinski's rule and the CMC-like rule, indicate that coumarins **2–4**, and **6** are suitable materials for future drug development.

3. Conclusion

The present study is the first to report the inhibitory activities of coumarins **2** and **3** on *h*MAOs and their enzyme kinetic properties. We confirmed *in vitro* anti-*h*MAO activity via an *in silico* hydrated molecular docking study and established structure–activity relationships for coumarins **1–6**, which have different functional groups in the umbelliferone scaffold. Our molecular docking results showed that coumarins **2** and **3** docked well into the active sites of *h*MAO-A and B and interacted with SBS residues via water-mediated hydrogen bonds and pi-pi stacked interactions. In particular, the formyl moiety in the C6 position of the umbelliferone scaffold interacted strongly with Tyr444 and Tyr197 of *h*MAO-A, whereas other functional moieties did not interact with the enzyme strongly enough to influence enzyme function. Moreover, coumarin **2** and **3** exhibited anti-lipid peroxidation activity in rat brain tissue and anti-$A\beta_{25\text{-}35}$ aggregation activity. The multifaceted nature of neuronal diseases has encouraged active development of multitarget-directed ligands that possess more than two complementary biological actions [44]. Taken together, formyl umbelliferones **2** and **3** are possible lead multitarget-directed ligands for the treatment of depression, as they have neuroprotective effects via inhibition of *h*MAO-A/B, self-Aβ aggregation, and lipid peroxidation. However, further studies in an animal model are needed to confirm our present findings and identify the underlying mechanism(s).

4. Materials and methods

4.1. Chemicals and reagents

*h*MAO isozymes, amyloid β-protein fragment 25–35 ($A\beta_{25\text{-}35}$), trolox, 1,1,1,3,3,3-hexafluoro-2-propanol, esculetin (purify > 97.5%)

Table 3
Molecular interactions of *h*MAO-B (2v5z) active site residues with coumarins **1–4** as well as reported inhibitors.

Compounds	Total binding energy[a]	H-bond interaction		Other interaction residues
		Direct	Water mediated	
1	−7.81	Cys172	Cys172	Tyr398 and Tyr435 (pi-pi stacked), FAD (pi-pi *T*-shaped)
2	−8.57	Cys172	Tyr188, Cys172	Tyr398 and Tyr435 (pi-pi stacked), FAD (pi-pi *T*-shaped, C–O bond), Leu171 and Ile198 (pi-alkyl), Cys172 (pi-sulfur), FAD (pi-lone pair)
3	−9.04	–	FAD, Thr399, Cys172, Tyr188	Tyr398 and Tyr435 (pi-pi Stacked), Leu171 (pi-alkyl), Cys172 (pi-sulfur)
4	−8.74	FAD	–	Tyr398 (pi-pi stacked), Leu171 (pi-alkyl), Cys172 (pi-sulfur)
Deprenyl[b]	−6.69	–	Ile198	Ile199 (pi-sigma), Tyr326 (pi-pi *T*-shaped), Tyr398 (pi-sigma), Ile171, Ile199, Tyr435, and FAD (pi-alkyl), Cys172 (pi-sulfur)
Safinamide[b]	−10.72	FAD, Gln206	–	Ile199 and Tyr326 (pi-pi *T*-shaped), Ile199, Ile316, Leu171, and Cys172 (pi-alkyl), Leu164 (halogen, F)

[a] Total binding energy (kcal/mol) of the hydrated inhibitor was calculated as the sum of normal ligand and W atom potentials.
[b] Reported inhibitors.

(**5**), scopoletin (purity > 99%) (**6**), and R-(–)-deprenyl HCl were purchased from Sigma-Aldrich (St. Louis, MO, USA). Sodium dodecyl sulfate (SDS) solution and thiobarbituric acid (TBA) were purchased from USB (Cleveland, OH, USA) and Tokyo Chemical Industry (Tokyo, Japan), respectively. All chemicals and solvents for column chromatography were of reagent grade from commercial sources and were used as received.

4.2. Preparation of umbelliferone derivatives

Umbelliferone (**1**), 6-formyl umbelliferone (**2**), and umbelliferone-6 carboxylic acid (**4**) were isolated from *Angelica decursiva* as described previously [17,23]. 8-Formyl umbelliferone (**3**) was synthesized from **1** following Qiao et al. [45]. Structures of the compounds were confirmed by ^{1}H- and ^{13}C NMR spectroscopy and compared with published data [17,23,46]. Purity of the compounds **1–4** was above 97%, as evidenced by spectral data. Compounds **5** and **6** were purchased from commercial vender as described above. Chemical structures of compounds **1–6** are shown in Table 1 and the assignment of ^{1}H- and ^{13}C NMR data of isolated (or synthesized) compounds **1–4** is shown in the supplementary information.

4.3. Human monoamine oxidases A and B enzyme assays

The MAO-Glo™ chemiluminescent assay kit (Promega, Madison, WI) was used to determine the inhibitory effects of compounds **1–6** against *h*MAO-A and *h*MAO-B. Each enzyme's activity was measured in arbitrary light units (ALU) in the presence of test samples and R-(–)-deprenyl HCl as a positive control. A 12.5 µL aliquot of a derivative of beetle luciferin (40 µM for *h*MAO-A and 4 µM for *h*MAO-B) was added to each well of a white opaque 96-well plate, followed by pre-incubation with 12.5 µL of one of the coumarins or the positive control at 25 ℃ for 5 min, and then 25 µL enzyme solution was added followed by a 1-hour incubation at 25 ℃. To terminate the enzymatic reaction and produce a luminescence signal, reconstituted luciferin detection reagent was added to each well. After 20 min, ALUs were measured using a VICTOR™ X multilabel reader (Perkin-Elmer, Wellesley, MA, USA).

4.4. Kinetic parameters of hMAO-A/B inhibition

Kinetic studies on the mechanism of *h*MAO-A and B inhibition by compounds **2** and **3** were conducted as described by Seong et al. [47]. Test concentrations of **2** and **3** used for the kinetic study are depicted in Figs. 2 and 3. The equations for the Lineweaver-Burk model are as follows:

$$1/V = K_m/V_{max}(1 + [I]/K_i)1/[S] + 1/V_{max}(1 + [I]/\alpha K_i).$$

A secondary plot can be constructed from

$$K_{m,app}/V_{max,app} = K_m[I]/K_i + K_m$$

$$1/V_{max,app} = 1/V_{max} + [I]/\alpha K_i V_{max}$$

where [S] and [I] denote the concentrations of MAO substrate and the tested compounds (**2** and **3**).

4.5. Hydrated docking simulations of hMAO-A and hMAO-B

Hydrated docking simulations were carried out with AutoDock 4.2 [48,49]. X-ray crystallographic structures of *h*MAO-A (2z5x) and *h*MAO-B (2v5z) were obtained from the RCSB Protein Data Bank (PDB) at resolutions of 2.2 and 1.6 Å [8,30], respectively. Water and ligand molecules were removed using Discovery Studio (v17.2, Accelrys, San Diego, CA, USA) except for FAD. Structures of coumarins **1–6** were generated and converted into 3D structures by Marvin Sketch (v17,1,30, ChemAxon, Budapest, Hungary). Structures of **1–6** were

Table 4
Inhibitory activity of coumarins on lipid peroxidation in rat brain homogenates and the formation of amyloid-β $(Aβ)_{25-35}$ fibrils.

Compound	Lipid peroxidation		Self-$Aβ_{25-35}$ aggregation	
	TBARS formation (nmol/mg protein)[a]	EC_{50} (μM)[b]	Thioflavin-T fluorescence[c]	IC_{50} (μM)[b]
Blank[d]	14.57 ± 1.06	–	–	–
Control	56.24 ± 2.27[#]	–	521.97 ± 10.12	–
1	55.21 ± 0.54	> 30	544.55 ± 12.57	> 100
2	14.73 ± 4.77[*]	8.98 ± 1.03	386.38 ± 10.41[*]	> 100
3	11.07 ± 0.41[*]	7.22 ± 1.67	183.87 ± 12.11[*]	75.57 ± 1.62
4	56.95 ± 2.45	> 30	475.7 ± 22.02	> 100
5	30.33 ± 2.86[*]	22.78 ± 4.42	495.04 ± 15.16	> 100
6	53.19 ± 4.77	> 30	524.57 ± 2.73	> 100
Trolox[e]	24.84 ± 0.27[*]	12.19 ± 0.11	–	–
Curcumin[c]	–	–	177.44 ± 2.03[*]	6.59 ± 0.27

[a] Mean ± SD ($n = 3$) at a concentration of 12.5 μM for tested coumarins and trolox.
[b] The 50% effective concentrations (EC_{50}) and 50% inhibition concentration (IC_{50}) are expressed as the mean ± SD, $n = 3$.
[c] Mean ± SD ($n = 3$) at a concentration of 100 μM for the tested coumarins and 10 μM for curcumin.
[d] Group without Fe^{2+} and TBA was used as a blank for the lipid peroxidation assay.
[e] Positive control.
[#] $p < 0.001$ indicates a significance difference from the blank.
[*] $p < 0.001$ indicates a significant difference from the control.

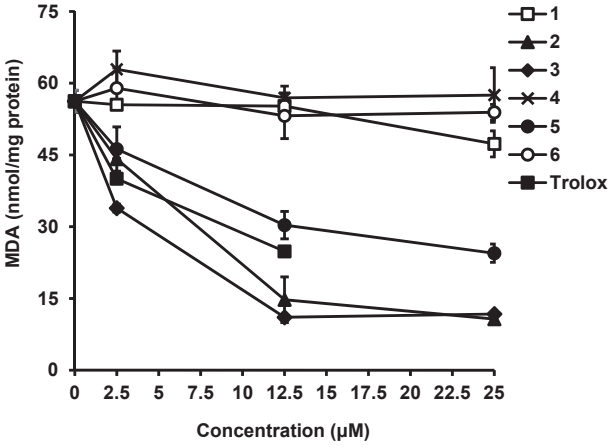

Fig. 5. Effects of coumarins on lipid peroxidation in whole rat brain homogenates. Trolox was used as the positive control. Data are presented as the mean ± SD.

energy-minimized using a molecular mechanics 2 (MM2) force field. Hydrated ligand and W maps were prepared according to a previous report [49]. For each coumarin (or standard)-*h*MAO complex, 10 docking poses were generated using the same docking parameters. The pose with the lowest binding energy in the most populated cluster was selected as the final hydrated docking result. Conserved W atoms were scored (strong or weak) and docking results were extracted. Docking results were visualized using Discovery Studio.

4.6. Self $Aβ_{25-35}$ aggregation assay

The $Aβ_{25-35}$ sample was prepared by Naldi's method [50]. A 2.5 μL aliquot of various concentrations of test compounds in 50 mM phosphate buffer (pH 7.4) with 100 mM NaCl was added to 100 μM $Aβ_{25-35}$ sample (72.5 μL) in Eppendorf tubes and the mixture was incubated at 4 ℃ for 24 h. After incubation, the reaction mixture was diluted with 675 μL of 25 μM thioflavin T in 50 mM glycine-NaOH buffer (pH 8.5). Fluorescence emission intensity was monitored at 490 nm ($λ_{exc}$ = 446 nm) using a fluorescence microplate reader (Gemini XPS, Molecular Devices, Sunnyvale, CA, USA).

4.7. Preparation of rat brain homogenate

Rat brain homogenates prepared from the whole brains of freshly killed six-month-old male Sprague Dawley rats were obtained from the Aging Tissue Bank of Pusan National University. Whole rat brains were homogenized in 10% weight per volume of cold 20 mM sodium phosphate buffer containing 140 mM potassium chloride (pH 7.4), and centrifuged at 1300*g* for 10 min. The supernatant fraction was used for the lipid peroxidation assay.

Table 5
ADME and drug-likeness characteristics of compounds **1–6**.

Pharmacokinetic properties		Compound					
		1	**2**	**3**	**4**	**5**	**6**
ADME	Log $P_{o/w}$[a]	1.44	1.44	1.19	1.60	1.54	1.68
	PPB[b]	42.39	81.58	54.96	83.93	11.47	29.42
	HIA[c]	94.17	93.11	93.11	83.64	88.20	93.92
	BBB penetration[d]	0.59	0.69	0.69	0.49	0.57	0.64
Drug-likeness	CMC-like rule	Not qualified	Qualified	Qualified	Qualified	Not qualified	Qualified
	Lipinski's rule	Suitable	Suitable	Suitable	Suitable	Suitable	Suitable

[a] The log of the coefficient for solvent partitioning between 1-octanol and water.
[b] < 90% indicates chemicals weakly bound and > 90% indicates chemicals strongly bound.
[c] 0–20% is poorly absorbed, 20–70% is moderately absorbed, and 70–100% is well absorbed.
[d] < 0.1 is low absorption by the central nervous system, 0.1–2.0 is moderate absorption, and > 2.0 is high absorption.

4.8. Lipid peroxidation assay

A thiobarbituric acid reactive species (TBARS) assay was used to evaluate the antioxidant activity of the coumarins in rat brain homogenates [51]. A 100 μL aliquot of the supernatant fraction of rat brain homogenates was incubated with various concentrations of coumarins or vehicle (50 μL), 30 μL of 250 μM freshly prepared ferric sulfate, and 120 μL of distilled water at 37 °C for 1 h. The reaction was terminated by adding 600 μL of 0.8% TBA, 300 μL of 8.1% SDS, and 600 μL of acetic acid (7.5% final)-NaOH solution (pH 3.4). The mixture was boiled at 100 °C for 1 h. After cooling, the mixture was extracted with *n*-butanol and centrifuged at 1300*g* for 5 min. The absorbance of the organic layer was measured at 532 nm using a spectrophotometer (Molecular Devices). TBARS formation was calculated from a calibration curve constructed using 1,1,3,3-tetramethoxypropane and expressed as MDA nmol/mg protein. Trolox was used as a positive control.

4.9. Prediction of pharmacokinetic parameters

PreADMET (http://preadmet.bmdrc.org) was used to investigate absorption, distribution, metabolism, excretion, toxicity (ADMET), and the drug-likeness properties of coumarins. Pharmacokinetic parameters evaluated in this study were log $P_{o/w}$, human intestinal absorption (HIA), plasma protein binding rate (PPB), and blood brain barrier permeability (BBB). The screening criteria for the ADMET properties are shown in Table 5.

4.10. Statistical analysis

The 50% inhibitory or effective concentration (IC_{50} or EC_{50}) values (μM) obtained from log dose inhibition curves are expressed as the mean ± SD (n = 3). Student's *t*-test (two-tailed) was used to calculate the significant differences between blank group and control group or sample treated group and control groups in the Table 4. Differences were considered as significant, when $p < 0.001$. All statistical analyses were achieved using Microsoft Excel 2016 Excel 2016 (Microsoft Corporation, Redmond, WA, USA).

Acknowledgments

This research was supported by the Basic Science Research Program through the National Research Foundation of Korea (Republic of Korea) funded by the Ministry of Science (2012R1A6A1028677). We also thank the Aging Tissue Bank (Pusan National University, Busan, Republic of Korea) for supplying rat brain tissue.

Declaration of Competing Interest

The authors have no conflicts of interest to declare.

Appendix A. Supplementary material

Supplementary data to this article can be found online at https://doi.org/10.1016/j.bioorg.2019.103293.

References

[1] A. Fonseca, J. Reis, T. Silva, M.J. Matos, D. Bagetta, F. Ortuso, S. Alcaro, E. Uriarte, F. Borges, Coumarin versus chromone monoamine oxidase B inhibitors: quo vadis? J. Med. Chem. 60 (2017) 7206–7212.
[2] J.P. Finberg, J.M. Rabey, Inhibitors of MAO-A and MAO-B in psychiatry and neurology, Front. Pharmacol. 7 (2016) 340.
[3] A.W. Bach, N.C. Lan, D.L. Johnson, C.W. Abell, M.E. Bembenek, S.W. Kwan, P.H. Seeburg, J.C. Shih, cDNA cloning of human liver monoamine oxidase A and B: molecular basis of differences in enzymatic properties, Proc. Natl. Acad. Sci. USA 85 (1988) 4934–4938.
[4] R.R. Ramsay, A. Albreht, Kinetics, mechanism, and inhibition of monoamine oxidase, J. Neural Transm. 125 (2018) 1659–1683.
[5] N. Pizzinat, N. Copin, C. Vindis, A. Parini, C. Cambon, Reactive oxygen species production by monoamine oxidases in intact cells, Naunyn Schmiedebergs Arch. Pharmacol. 359 (1999) 428–431.
[6] A. Maurel, C. Hernandez, O. Kunduzova, G. Bompart, C. Cambon, A. Parini, B. Frances, Age-dependent increase in hydrogen peroxide production by cardiac monoamine oxidase A in rats, Am. J. Physiol. Heart Circ. Physiol. 284 (2003) H1460–H1467.
[7] J.K. Mallajosyula, D. Kaur, S.J. Chinta, S. Rajagopalan, A. Rane, D.G. Nicholls, D.A. Di Monte, H. Macarthur, J.K. Andersen, MAO-B elevation in mouse brain astrocytes results in Parkinson's pathology, PloS one 3 (2008) e1616.
[8] S.Y. Son, J. Ma, Y. Kondou, M. Yoshimura, E. Yamashita, T. Tsukihara, Structure of human monoamine oxidase A at 2.2-Å resolution: the control of opening the entry for substrates/inhibitors, Proc. Natl. Acad. Sci. USA 105 (2008) 5739–5744.
[9] M. Yamada, H. Yasuhara, Clinical pharmacology of MAO inhibitors: safety and future, Neurotoxicology 25 (2004) 215–221.
[10] Y. Bandaruk, R. Mukai, T. Kawamura, H. Nemoto, J. Terao, Evaluation of the inhibitory effects of quercetin-related flavonoids and tea catechins on the monoamine oxidase-A reaction in mouse brain mitochondria, J. Agric. Food Chem. 60 (2012) 10270–10277.
[11] D.R. de Oliveira, L.F. Schaffer, A. Busanello, C.P. Barbosa, L.R. Peroza, C.M. de Freitas, B.N. Krum, G.N. Bressan, A.A. Boligon, M.L. Athayde, I.R.A. de Menezes, R. Fachinetto, Silymarin has antioxidant potential and changes the activity of Na^+/K^+-ATPase and monoamine oxidase in vitro, Ind. Crops Prod. 70 (2015) 347–355.
[12] Y. Song, P. Li, L. Liu, C. Bortolini, M. Dong, Nanostructural differentiation and toxicity of amyloid-beta25-35 aggregates ensue from distinct secondary conformation, Sci. Rep. 8 (2018) 765.
[13] G. Oboh, A.O. Ademiluyi, O.B. Ogunsuyi, S.I. Oyeleye, A.F. Dada, A.A. Boligon, Cabbage and cucumber extracts exhibited anticholinesterase, antimonoamine oxidase and antioxidant properties, J. Food Biochem. 41 (2017) e12358.
[14] C. Pike, D. Burdick, A. Walencewicz, C. Glabe, C. Cotman, Neurodegeneration induced by β-amyloid peptides *in vitro*: the role of peptide assembly state, J. Neurosci. 13 (1993) 1676–1687.
[15] K.N. Venugopala, V. Rashmi, B. Odhav, Review on natural coumarin lead compounds for their pharmacological activity, Biomed. Res. Int. 2013 (2013) 963248.
[16] A.M. Holbrook, J.A. Pereira, R. Labiris, H. McDonald, J.D. Douketis, M. Crowther, P.S. Wells, Systematic overview of warfarin and its drug and food interactions, Arch. Intern. Med. 165 (2005) 1095–1106.
[17] D. Zhao, M. Nurul Islam, B.R. Ahn, H.A. Jung, B.W. Kim, J.S. Choi, *In vitro* antioxidant and anti-inflammatory activities of *Angelica decursiva*, Arch. Pharm. Res. 35 (2012) 179–192.
[18] R.A. Newman, W. Chen, T.L. Madden, Pharmaceutical properties of related calanolide compounds with activity against human immunodeficiency virus, J. Pharm. Sci. 87 (1998) 1077–1080.
[19] K. Skalicka-Wozniak, I.E. Orhan, G.A. Cordell, S.M. Nabavi, B. Budzynska, Implication of coumarins towards central nervous system disorders, Pharmacol. Res. 103 (2016) 188–203.
[20] S. Emami, S. Dadashpour, Current developments of coumarin-based anti-cancer agents in medicinal chemistry, Eur. J. Med. Chem. 102 (2015) 611–630.
[21] J.C. Capra, M.P. Cunha, D.G. Machado, A.D. Zomkowski, B.G. Mendes, A.R. Santos, M.G. Pizzolatti, A.L. Rodrigues, Antidepressant-like effect of scopoletin, a coumarin isolated from Polygala sabulosa (Polygalaceae) in mice: evidence for the involvement of monoaminergic systems, Eur. J. Pharmacol. 643 (2010) 232–238.
[22] S.R. Subramaniam, E.M. Ellis, Neuroprotective effects of umbelliferone and esculetin in a mouse model of Parkinson's disease, J. Neurosci. Res. 91 (2013) 453–461.
[23] M.Y. Ali, S.H. Seong, M.R. Reddy, S.Y. Seo, J.S. Choi, H.A. Jung, Kinetics and molecular docking studies of 6-formyl umbelliferone isolated from angelica decursiva as an inhibitor of cholinesterase and BACE1, Molecules 22 (2017) 1604.
[24] T. Qin, F. Fang, M. Song, R. Li, Z. Ma, S. Ma, Umbelliferone reverses depression-like behavior in chronic unpredictable mild stress-induced rats by attenuating neuronal apoptosis via regulating ROCK/Akt pathway, Behav. Brain Res. 317 (2017) 147–156.
[25] C. Gnerre, M. Catto, F. Leonetti, P. Weber, P.A. Carrupt, C. Altomare, A. Carotti, B. Testa, Inhibition of monoamine oxidases by functionalized coumarin derivatives: biological activities, QSARs, and 3D-QSARs, J. Med. Chem. 43 (2000) 4747–4758.
[26] C. Mattsson, P. Svensson, C. Sonesson, A novel series of 6-substituted 3-(pyrrolidin-1-ylmethyl)chromen-2-ones as selective monoamine oxidase (MAO) A inhibitors, Eur. J. Med. Chem. 73 (2014) 177–186.
[27] S.H. Jeong, X.H. Han, S.S. Hong, J.S. Hwang, J.H. Hwang, D. Lee, M.K. Lee, J.S. Ro, B.Y. Hwang, Monoamine oxidase inhibitory coumarins from the aerial parts of *Dictamnus albus*, Arch. Pharm. Res. 29 (2006) 1119–1124.
[28] S.J. Lee, H.Y. Chung, I.K. Lee, S.U. Oh, I.D. Yoo, Phenolics with inhibitory activity on mouse brain monoamine oxidase (MAO) from whole parts of *Artemisia vulgaris* L (Mugwort), Food Sci. Biotechnol. 9 (2000) 179–182.
[29] H. Kim, S.O. Sablin, R.R. Ramsay, Inhibition of monoamine oxidase A by β-carboline derivatives, Arch. Biochem. Biophys. 337 (1997) 137–142.
[30] C. Binda, J. Wang, L. Pisani, C. Caccia, A. Carotti, P. Salvati, D.E. Edmondson, A. Mattevi, Structures of human monoamine oxidase B complexes with selective noncovalent inhibitors: safinamide and coumarin analogs, J. Med. Chem. 50 (2007) 5848–5852.
[31] R.M. Geha, K. Chen, J. Wouters, F. Ooms, J.C. Shih, Analysis of conserved active site residues in monoamine oxidase A and B and their three-dimensional molecular modeling, J. Biol. Chem. 277 (2002) 17209–17216.
[32] R.M. Geha, I. Rebrin, K. Chen, J.C. Shih, Substrate and inhibitor specificities for human monoamine oxidase A and B are influenced by a single amino acid, J. Biol. Chem. 276 (2001) 9877–9882.
[33] R.P. Weinberg, V.V. Koledova, H. Shin, J.H. Park, Y.A. Tan, A.J. Sinskey,

R. Sambanthamurthi, C. Rha, Oil palm phenolics inhibit the *in vitro* aggregation of β-amyloid peptide into oligomeric complexes, Int. J. Alzheimers Dis. 2018 (2018) 7608038.
[34] J.M. Braughler, L.A. Duncan, R.L. Chase, The involvement of iron in lipid peroxidation. Importance of ferric to ferrous ratios in initiation, J. Biol. Chem. 261 (1986) 10282–10289.
[35] P.T. Thuong, T.M. Hung, T.M. Ngoc, T. Ha do, B.S. Min, S.J. Kwack, T.S. Kang, J.S. Choi, K. Bae, Antioxidant activities of coumarins from Korean medicinal plants and their structure-activity relationships, Phytother. Res. 24 (2010) 101–106.
[36] S. Singh, J. Singh, Transdermal drug delivery by passive diffusion and iontophoresis: A review, Med. Res. Rev. 13 (1993) 569–621.
[37] S. Yee, In vitro permeability across Caco-2 cells (colonic) can predict in vivo (small intestinal) absorption in man - fact or myth, Pharm. Res. 14 (1997) 763–766.
[38] X.L. Ma, C. Chen, J. Yang, Predictive model of blood-brain barrier penetration of organic compounds, Acta Pharmacol. Sin. 26 (2005) 500–512.
[39] F. Zhang, J. Xue, J. Shao, L. Jia, Compilation of 222 drugs' plasma protein binding data and guidance for study designs, Drug Discov. Today 17 (2012) 475–485.
[40] Y.H. Zhao, J. Le, M.H. Abraham, A. Hersey, P.J. Eddershaw, C.N. Luscombe, D. Butina, G. Beck, B. Sherborne, I. Cooper, J.A. Platts, Evaluation of human intestinal absorption data and subsequent derivation of a quantitative structure-activity relationship (QSAR) with the Abraham descriptors, J. Pharm. Sci. 90 (2001) 749–784.
[41] A.K. Ghose, V.N. Viswanadhan, J.J. Wendoloski, A knowledge-based approach in designing combinatorial or medicinal chemistry libraries for drug discovery. 1. A qualitative and quantitative characterization of known drug databases, J. Comb. Chem. 1 (1999) 55–68.
[42] C.A. Lipinski, F. Lombardo, B.W. Dominy, P.J. Feeney, Experimental and computational approaches to estimate solubility and permeability in drug discovery and development settings, Adv. Drug Deliv. Rev. 23 (1997) 3–25.
[43] X. Liu, M. Wright, C.E. Hop, Rational use of plasma protein and tissue binding data in drug design, J. Med. Chem. 57 (2014) 8238–8248.
[44] L. Huang, C. Lu, Y. Sun, F. Mao, Z. Luo, T. Su, H. Jiang, W. Shan, X. Li, Multitarget-directed benzylideneindanone derivatives: anti-β-amyloid (Aβ) aggregation, antioxidant, metal chelation, and monoamine oxidase B (MAO-B) inhibition properties against Alzheimer's disease, J. Med. Chem. 55 (2012) 8483–8492.
[45] Y. Qiao, B. Chen, Y. Yang, X. Wang, Y. Xu, H. Li, Rational design of a highly selective fluorescent sensor for L-histidine detection in aqueous solution, Dalton Trans. 45 (2016) 1310–1314.
[46] S. Caffieri, F. Di Lisa, F. Bolesani, M. Facco, G. Semenzato, F. Dall'Acqua, M. Canton, The mitochondrial effects of novel apoptogenic molecules generated by psoralen photolysis as a crucial mechanism in PUVA therapy, Blood 109 (2007) 4988–4994.
[47] S.H. Seong, M.T. Ha, B.S. Min, H.A. Jung, J.S. Choi, Moracin derivatives from Morus Radix as dual BACE1 and cholinesterase inhibitors with antioxidant and anti-glycation capacities, Life Sci. 210 (2018) 20–28.
[48] D.S. Goodsell, G.M. Morris, A.J. Olson, Automated docking of flexible ligands: applications of autodock, J. Mol. Recognit. 9 (1996) 1–5.
[49] S. Forli, A.J. Olson, A force field with discrete displaceable waters and desolvation entropy for hydrated ligand docking, J. Med. Chem. 55 (2012) 623–638.
[50] M. Naldi, J. Fiori, M. Pistolozzi, A.F. Drake, C. Bertucci, R. Wu, K. Mlynarczyk, S. Filipek, A. De Simone, V. Andrisano, Amyloid β-peptide 25–35 self-assembly and its inhibition: a model undecapeptide system to gain atomistic and secondary structure details of the Alzheimer's disease process and treatment, ACS Chem. Neurosci. 3 (2012) 952–962.
[51] H. Ohkawa, N. Ohishi, K. Yagi, Assay for lipid peroxides in animal tissues by thiobarbituric acid reaction, Anal. Biochem. 95 (1979) 351–358.